

Adsorption and hydrogenation of pyridine and pyrrole on NiMoS: an ab initio density-functional theory study

Mingyong Sun^a, Alan E. Nelson^{a,*}, John Adjaye^b

^a University of Alberta, Department of Chemical and Materials Engineering, Edmonton, AB, Canada T6G 2G6

^b Syncrude Canada Ltd., Edmonton Research Centre, Edmonton, AB, Canada T6N1H4

Received 1 December 2004; revised 14 January 2005; accepted 18 January 2005

Abstract

The adsorption and first-step hydrogenation of pyridine and pyrrole on the Ni-promoted (10 $\bar{1}$ 0) edge of MoS₂ are studied with the use of periodic density-functional theory calculations under generalized gradient approximation. This study represents the first systematic theoretical investigation of the energetics and reaction pathways of possible reaction mechanisms (Langmuir–Hinshelwood, Eley–Rideal) for the hydrogenation of pyridine and pyrrole on the NiMoS catalyst edge plane. The most stable configuration for adsorbed pyridine on the Ni-edge surface is with the molecular plane perpendicular to the surface through N–Ni bonding. Pyrrole preferably interacts with the surface through the bonding of an α -carbon to a nickel site with the molecular plane flat on the surface. For the hydrogenation of pyridine via a Langmuir–Hinshelwood mechanism, the lowest-activation-energy reaction pathway involves hydrogen from adsorbed H₂S; for pyrrole the lowest-activation-energy reaction pathway involves hydrogen from the –SH groups at the edge of the MoS₂ (0001) basal plane. Eley–Rideal reaction pathways involving gas-phase pyridine or pyrrole and surface hydrogen species require very low activation energy, and thus the dissociation of hydrogen on the catalyst surface would be the rate-determining step under these reaction conditions.

© 2005 Elsevier Inc. All rights reserved.

Keywords: Pyridine; Pyrrole; Adsorption; Hydrodenitrogenation; Hydrogenation; Density-functional theory

1. Introduction

Hydrotreating is one of the most important industrial catalytic processes, whereby sulfur and nitrogen are removed from petroleum fractions to meet transportation fuel environmental regulations. The increasing interest in upgrading of heavy oils and vacuum residue, which have higher sulfur and nitrogen content compared with conventional crude oils continues to drive the research and development of new hydrotreating catalysts with higher activity and selectivity.

Hydrotreating catalysts currently used in upgrading and refining are typically composed of nickel (or cobalt) and molybdenum supported on γ -Al₂O₃, which are prepared in an oxidic state and converted to a sulfidic state before

use [1,2]. The incorporation of cobalt and nickel into molybdenum sulfide catalysts results in much higher activities than corresponding monometallic molybdenum, cobalt, or nickel sulfide catalysts. The promotional effect of cobalt (or nickel) in the promoted molybdenum sulfide catalysts has been attributed to the formation of the so-called CoMoS (or NiMoS) phase proposed by Topsøe et al. [3]. The structure of the CoMoS (or NiMoS) phase has been a topic of many studies, and a clear picture of the CoMoS (or NiMoS) phase has emerged because of combinational efforts of experimental and theoretical studies [4–9].

Molybdenum exists as MoS₂ clusters in Mo-based sulfide catalysts. With Co (or Ni)-promoted molybdenum sulfide catalysts, the promoter atoms are located at the edge planes of the MoS₂ *hcp* layered structure by replacement of the molybdenum atoms on either the (1 $\bar{1}$ 0) or (10 $\bar{1}$ 0) edge planes. Under typical sulfidation conditions, cobalt prefers to replace molybdenum on the (1 $\bar{1}$ 0) S-edge and nickel

* Corresponding author. Fax: +1 780 492 2881.

E-mail address: alan.nelson@ualberta.ca (A.E. Nelson).

tends to replace molybdenum on the $(10\bar{1}0)$ Mo-edge [4–9]. The incorporation of the promoter atoms decreases the binding energy of sulfur on the edge planes, thus reducing the equilibrium sulfur coverage on respective edge surfaces of promoted MoS_2 catalysts [5–9]. The fully nickel-substituted edge plane (Ni-edge) tends to be uncovered by sulfur, and the unpromoted Mo-edge is covered by sulfur in a bridging position under typical reaction conditions [6–8].

Understanding the details of the HDN reaction mechanism on the catalyst surface is an essential part of catalysis research, which provides further insight into the nature of active sites on catalysts and intrinsic activation energies for specific surface reactions at the atomic level. Whereas the salient features of the hydrodenitrogenation process have been studied by characterization of the intermediates detectable in bulk reacting fluids, the mechanisms and energetics of organonitrogen hydrogenation and C–N bond scission on the stable edge surfaces of MoS_2 -based catalysts are poorly understood [10,11]. Surface science studies have elucidated the adsorption modes and energetics of pyridine [12–14] and pyrrole [15–17] on various model surfaces. However, the details and energetics of the elementary reactions on the model surfaces remain unclear, and no study has been reported for the adsorption and reaction of pyridine and pyrrole on the Ni-edge surface of the NiMoS catalyst.

To further understand HDN mechanisms of basic and nonbasic nitrogen compounds on MoS_2 -based catalyst surfaces, additional studies on the adsorption and reactions of nitrogen compounds on the edge surfaces of NiMoS are required. Therefore, the present study investigates the adsorption and first-step hydrogenation energetics of pyridine and pyrrole on NiMoS with the use of density-functional theory (DFT) to elucidate hydrogenation pathways and rate-controlling events. The adsorption geometries of these molecules on nickel-promoted MoS_2 $(10\bar{1}0)$ edge surfaces are summarized, and the possible reaction mechanisms for the first-step hydrogenation are subsequently presented and discussed based on the identified adsorption configurations and relative energetics. This study represents the first systematic theoretical investigation of the energetics and reaction pathways of possible reaction mechanisms (Langmuir–Hinshelwood, Eley–Rideal) for the hydrogenation of pyridine and pyrrole on the $(10\bar{1}0)$ edge plane of NiMoS.

2. Methods

2.1. Catalyst models

The NiMoS catalyst model used in the present study is shown in Fig. 1, in which the molybdenum atoms on the $(10\bar{1}0)$ edge surface have been replaced by nickel atoms to obtain the fully nickel-promoted catalyst surface, termed the Ni-edge [8]. The model is repeated in the x direction with a periodicity of six MoS_2 units, and separated by vacuum layers of 15 Å in the y and z directions with a corresponding su-

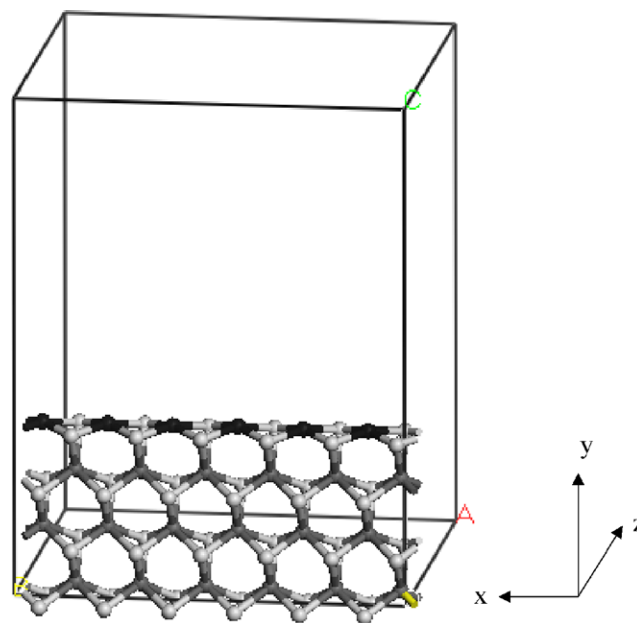


Fig. 1. Catalyst model. Black: nickel, dark grey: molybdenum, light grey: sulfur.

percell volume of $19.0 \times 24.6 \times 18.4$ Å. The large supercell prevents the interaction between adsorbates (pyridine or pyrrole) in neighboring cells, which may affect the adsorption geometry or reaction energetics. Adsorption and dissociation of hydrogen sulfide and hydrogen on the Ni-edge surface used to generate surface hydrogen species have been investigated in our previous work [18]. The adsorbed H_2S , Ni–H, and –SH groups are identified as the stable hydrogen species on the Ni-edge, which are considered as the possible sources of hydrogen for the hydrogenation of pyridine and pyrrole in the present study.

2.2. DFT calculations

The energy calculations are based on density-functional theory (DFT) and have been performed with the use of Materials Studio DMol³ from Accelrys® (version 2.2) [19]. The double-numerical plus polarization functions (DNP) and Becke exchange [20] plus Perdew–Wang approximation [21] nonlocal functionals (GGA-PW91) are used in all calculations. The real space cutoff radius is 4.5 Å. All electron basis sets are used for light elements, such as hydrogen, oxygen, and sulfur. Effective Core Potentials [22,23] are used to treat core electrons of molybdenum and nickel, and a k -point of $(1 \times 1 \times 1)$ was used because of the large supercell. Spin polarization was applied to all calculations for the systems containing nickel. The same methodology has been used previously in the calculation of the adsorption and dissociation of hydrogen on the NiMoS catalyst surface [18]. To determine the activation energy for a specific reaction path, a transition state that connects two immediate stable structures through a minimum energy path was identified by complete synchronous transit (LST) and quadratic syn-

chronous transit (QST) search methods [24,25] followed by transition-state confirmation through the nudged elastic band (NEB) method [26].

3. Results and discussion

3.1. Adsorption of pyridine and pyrrole on the Ni-edge surface

In nickel-promoted molybdenum sulfide catalysts, nickel atoms prefer to incorporate into the MoS₂ structure by replacing molybdenum atoms at the (10 $\bar{1}$ 0) edge of MoS₂, thereby generating the so-called Ni-edge surface as shown in Fig. 1 [8,18]. In the following discussions, the adsorption and reactions of molecules occur on such a Ni-edge surface including six nickel atoms in a supercell; however, only a portion of the Ni-edge is shown to display different surface configurations of molecules on the surface.

3.1.1. Pyridine adsorption

On the Ni-edge, the adsorption of pyridine can be side-on with the pyridine plane parallel to the Ni-edge surface plane, or end-on with the molecular plane perpendicular to the Ni-edge plane. In each mode, the molecule can be directly atop a nickel site or between two nickel sites at a bridge location. Table 1 summarizes several adsorption configurations for pyridine on the Ni-edge and corresponding adsorption energies. For the side-on configurations, the N–C₄ axis of pyridine can be along (Schemes 1a and b) or across (Schemes 1c and d) the nickel plane. The center of the pyridine ring is positioned between two nickel sites for Schemes 1a and c, and on top of a nickel site for Schemes 1b and d. For the end-on adsorption, the most stable configuration is with the pyridinic nitrogen bonding to a nickel site

directly atop, which can be explained by the electronic orbital configuration of pyridine [27]. The optimized geometry and adsorption energy are the same as in Scheme 1a when the molecule is originally placed on the surface end-on (not shown).

The adsorption energies listed in Table 1 are calculated based on the differences in electronic energies between the adsorption complex and a clean surface plus gas-phase pyridine. The configurations with the ring center atop a nickel site always lead to lower adsorption energies. It is interesting to note that when the pyridinic nitrogen is close enough to a nickel site, regardless of whether the initial configuration is side-on or end-on, the optimized configuration for the adsorbed pyridine is always end-on atop the nickel site (Scheme 1a, optimized). The end-on adsorption through N–Ni bonding generates a larger adsorption energy (1.29 eV, 1 eV = 96.485 kJ mol⁻¹) than side-on adsorption (0.26 eV).

The hydrogenation of pyridine occurs before C–N bond cleavage [10,11,28–32]. Side-on configurations would allow pyridine to directly interact with the surface through π -electrons and thus activate the aromatic ring system for hydrogenation. Following this argument, several other possible configurations with different carbon atoms interacting with the catalyst surface were studied (not shown). However, Scheme 1c produced the largest adsorption energy and interaction with the catalyst surface for the side-on configurations. The lower adsorption energies for side-on configurations do not indicate a strong interaction between pyridine and the catalyst surface.

The interatomic bond distances in pyridine before and after adsorption for Schemes 1a–d are presented in Table 2. The C–N bond for end-on adsorption and the C₂–C₃ bond for side-on adsorption are only slightly longer than that for gas-phase pyridine. In general, pyridine deforms only slightly upon adsorption, and thus the molecule is not activated to a significant extent upon adsorption on the Ni-edge

Table 1
Surface configurations of pyridine on the Ni-edge surface before and after optimization, and the relative energies of optimized configurations with the clean surface and gas-phase pyridine as energetic references

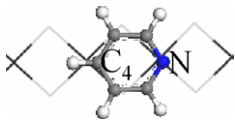
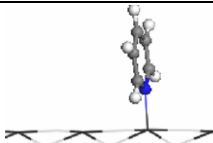
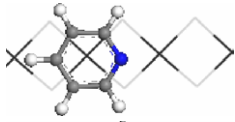
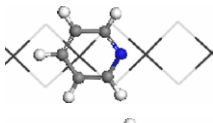
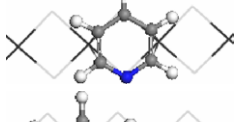
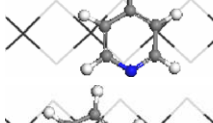
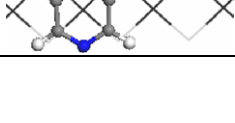
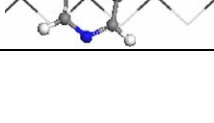
Scheme	Initial	Optimized	Adsorption energy (eV)
1a			-1.29
1b			-0.10
1c			-0.26
1d			-0.15

Table 2
Bond distances in gas-phase pyridine and adsorbed pyridine on the Ni-edge

State of pyridine	Bond distance (Å)		
	N–C ₂	C ₂ –C ₃	C ₃ –C ₄
Free	1.343	1.397	1.396
Scheme 1a	1.350	1.391	1.395
Scheme 1b	1.337	1.405	1.400
Scheme 1c	1.342	1.404	1.399
Scheme 1d	1.342	1.399	1.397

surface. Although end-on adsorption is associated with a larger adsorption energy, this bonding mode does not affect the aromaticity of pyridine.

3.1.2. Pyrrole adsorption

The end-on adsorption through a N–Ni bond is impossible for pyrrole because of its electronic structure [27]. For side-on adsorption, the ring center of pyrrole is either initially placed above a nickel site or between two nickel sites with different orientations, as was done for pyridine. After optimization, the ring center of pyrrole prefers the bridge location between two nickel sites, and the nitrogen atom tends to move away from the Ni-edge catalyst surface.

The interaction between pyrrole and the Ni-edge surface preferably occurs through carbon atoms rather than the nitrogen atom. Table 3 presents two representative optimized configurations with the α (C₂ or C₅) and β (C₃ or C₄) car-

Table 4
Bond distances in gas-phase pyrrole and adsorbed pyrrole on the Ni-edge

State of pyrrole	Bond distance (Å)				
	N–C ₂	C ₂ –C ₃	C ₃ –C ₄	C ₄ –C ₅	C ₅ –N
Free	1.377	1.382	1.424	1.382	1.377
Scheme 3a	1.391	1.375	1.436	1.410	1.353
Scheme 3b	1.402	1.416	1.404	1.399	1.350

bon atoms bonding to a nickel site. The configuration with an α -C bonding to a nickel site has a slightly larger adsorption energy (Scheme 3b) than one with a β -C (Scheme 3a) bonding to a nickel site. These results indicate that the adsorption of pyrrole on the Ni-edge surface preferentially occurs through a α -C and Ni site interaction. Table 4 summarizes the bond distances of gas-phase and adsorbed pyrrole. Upon adsorption, pyrrole is significantly deformed. In Scheme 3b, N–C₂, C₂–C₃, and C₄–C₅ bond distances are increased, and the other bond distances are decreased. The significant changes in bond distances of adsorbed pyrrole indicate the strong activation of the molecule on the catalyst surface.

3.2. Hydrogenation of pyridine

3.2.1. Energetics of noncatalytic pyridine hydrogenation

As a reference, the energy profile for noncatalytic pyridine hydrogenation was calculated. Table 5 gives the relative energetics of possible intermediate species with different

Table 3
Surface configurations of pyrrole on the Ni-edge surface after optimization, and the relative energies of optimized configurations with the clean surface and gas-phase pyrrole as energetic references

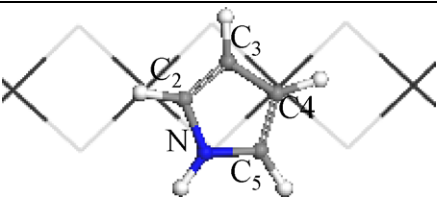

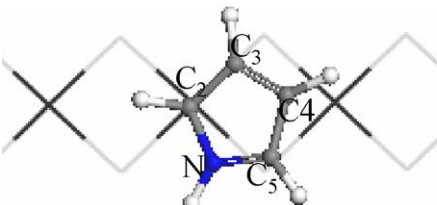
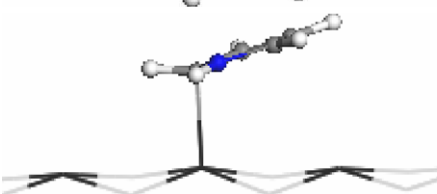
Scheme	Optimized geometry	Adsorption energy (eV)
3a	Top view 	–0.68
	Side view 	
3b	Top view 	–0.71
	Side view 	

Table 5
Relative energies of gas-phase pyridine hydrogenation with pyridine and molecular hydrogen as energetic references

State of pyridine	Relative energy (eV)
Pyridine	0
Monohydrogen pyridine	
1-MHpyridine	0.73
2-MHpyridine	1.11
3-MHpyridine	1.10
4-MHpyridine	1.12
Dihydrogen pyridine	
1,2-DHpyridine	0.02
2,3-DHpyridine	0.10
3,4-DHpyridine	0.08
Trihydrogen pyridine	
1,2,3-Trihydrogen pyridine	0.09
2,3,4-Trihydrogen pyridine	0.07
Tetrahydrogen pyridine	
1,2,3,4-Tetrahydrogen pyridine	-1.39
2,3,4,5-Tetrahydrogen pyridine	-1.33
Pentahydrogen pyridine	
1,2,3,4,5-Pentahydrogen pyridine	-0.68
2,3,4,5,6-Pentahydrogen pyridine	-0.54
Piperidine	-2.68

degrees of hydrogenation with gas-phase pyridine and molecular hydrogen as energy references. For monohydrogenation, the relative energy of N-MHpyridine (1-MHpyridine) is much lower than that of the other three MHpyridines. In N-MHpyridine, the hydrogen bonds to the nitrogen atom of pyridine through its lone pair electrons and not the π -electrons. The aromatic ring structure is not significantly affected by monohydrogenation. For dihydrogenation, 1,2-DHpyridine is more stable than 2,3 and 3,4 isomers; other dihydrogenation products, such as 2,6- and 3,5-DHpyridines, have much higher energies and are much less stable. The addition of an even number of hydrogen atoms, from monohydrogenation to dihydrogenation and from trihydrogenation to tetrahydrogenation, is always an exothermic process. For example, the reaction energy from 1-MHpyridine to 1,2-DHpyridine is -0.71 eV, and from 1,2,3-trihydrogenation to 1,2,3,4-tetrahydrogenation it is -1.48 eV (Table 5). On the other hand, the first and fifth steps of hydrogenation are endothermic processes. The reaction energy is 0.73 eV from pyridine to 1-MHpyridine and 0.74 eV from 1,2,3,4-tetrahydrogenation to 1,2,3,4,5-pentahydrogenation (Table 5). For the hydrogenation of pyridine to occur, molecular hydrogen must dissociate to active hydrogen atoms. This gas-phase dissociation requires 4.52 eV/ H_2 . After dissociation, the active hydrogen atoms react with pyridine. The reaction between a pyridine molecule and a hydrogen atom to monohydrogenation can readily occur ($E_a < 0.1$ eV). Therefore, the rate-determining step for gas-phase hydrogenation is the dissociation of molecular hydrogen.

3.2.2. Mechanism and energetics of catalytic pyridine hydrogenation on the Ni-edge

Numerous experimental studies of HDN kinetics have assumed that the reactions proceed via the Langmuir–

Hinshelwood (L-H) mechanism, which indicates that the reaction takes place between chemisorbed pyridine and hydrogen species [28–32]. The results of Section 3.1 show that the side-on adsorption of pyridine on the Ni-edge surface does not significantly change the structure of pyridine with a relatively low adsorption energy (0.26 eV). Therefore, it is unlikely that side-on adsorption would facilitate pyridine hydrogenation to a significant extent. The end-on adsorption of pyridine involves the formation of a Ni–N bond with a large adsorption energy (1.29 eV); therefore, the end-on adsorption would be the dominant configuration for pyridine on the catalyst surface. Thus, the HDN of pyridine via a L-H mechanism is assumed to occur between surface hydrogen species and end-on adsorbed pyridine. Depending on the partial pressure of H_2 and H_2S in the gas phase, different surface hydrogen species are present on the catalyst surface through adsorption and dissociation of H_2 and H_2S [18]. Accordingly, different hydrogen species are considered in the following mechanistic and energetic discussions.

In the first mechanism, adsorbed H_2S is considered as the source of hydrogen for hydrogenation, which is the most stable hydrogen species on the Ni-edge surface [18]. As indicated by Schemes 6a and b in Table 6, one hydrogen atom from the adsorbed H_2S is added to an adsorbed pyridine at the neighbor site. When the hydrogen is added to an α -C of pyridine to form 2-MHpyridine (Scheme 6a), the nitrogen atom remains bound to the nickel site. This path requires an activation energy of 1.5 eV and results in a reaction energy of 1.3 eV. As shown in Table 5, N-MHpyridine is more stable than 2-MHpyridine as free gas-phase molecules. In Scheme 6b, the nitrogen may break the bond with the nickel site to abstract a hydrogen atom from the adsorbed H_2S , in which hydrogen has a protonic property. The formation of N-MHpyridine only requires an activation energy of 0.6 eV and a reaction energy of 0.3 eV. These results indicate that N-MHpyridine is much more stable and that its formation is much easier compared with 2-MHpyridine on the NiMoS catalyst surface.

Molecular hydrogen may also dissociate on the Ni-edge surface to form two Ni–H groups, or a Ni–H group and a –SH group with a sulfur atom on the basal plane [18]. In Schemes 6c and d (Table 6), the reaction is initiated with an adsorbed pyridine and a Ni–H and –SH pair. The reaction requires a lower activation energy when the hydrogen is from the –SH than when it is from the Ni–H. When there are only Ni–H groups on the surface, the hydrogen atoms would most likely migrate from Ni–H to a sulfur atom at basal plane to form an –SH group closer to the adsorbed pyridine. The reaction would then occur between the –SH and the adsorbed pyridine. Again, the formation of 2-MHpyridine (Scheme 6c) is thermodynamically and kinetically less favorable than that of N-MHpyridine (Scheme 6d) when the hydrogen is from an –SH group at basal plane.

In summary, the L-H mechanisms studied indicate that the reaction paths involving adsorbed H_2S (Schemes 6a and b) always have lower activation energies than those in-

Table 6
Activation and reaction energies of various reaction paths for the monohydrogenation of adsorbed pyridine via the Langmuir–Hinshelwood mechanism

Reaction path	Reactant	Transition state	Product
Scheme 6a			
Relative energy (eV)	0	1.5	1.3
Scheme 6b			
Relative energy (eV)	0	0.6	0.3
Scheme 6c			
Relative energy (eV)	0	2.2	0.6
Scheme 6d			
Relative energy (eV)	0	1.3	0.1

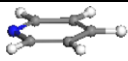
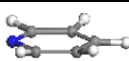
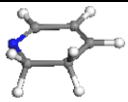

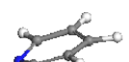
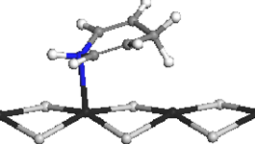
volving the Ni–H or basal plane –SH (Schemes 6c and d) for the first-step monohydrogenation of pyridine.

Another possible mechanism involves reactions between gas-phase and chemisorbed species, which is referred to as an Eley–Rideal (E-R) mechanism. Although this type of reaction mechanism has not been used in interpreting HDN experimental data, hydrogenation may proceed via an E-R mechanism at certain reaction conditions. For example, at very low partial pressures of pyridine and very high partial pressures of hydrogen, the Ni-edge catalyst surface would be covered by a significant amount of Ni–H [18], thus facilitating the reaction between gas-phase pyridine and adsorbed surface hydrogen species. When gas-phase pyridine approaches a Ni-edge surface, on which some sites are covered by nickel hydrides and some are uncovered, the pyridine may interact either with the uncovered nickel sites or with Ni–H. Both paths are exothermic processes and require no activation energy. Table 7 shows the relative energies of the two possible surface configurations relative to gas-phase pyridine and surface hydrides. When a significant number of vacant nickel sites are available on the Ni-edge surface, the adsorption of pyridine on the nickel sites would dominate over the direct formation of N–MHpyridine. The reaction

Table 7
Relative stabilities of adsorbed pyridine on the nickel site with neighboring Ni–H and the N-monohydropyridine by the Ni–H

Scheme	Optimized geometry	Relative energy (eV)
7a		0
7b		–1.0
7c		–1.3

Table 8
Activation and reaction energies of various reaction paths for dihydrogenation of pyridine via the Eley–Rideal mechanism

Reaction path	Reactant	Transition state	Product
Scheme 8a			
Relative energy (eV)	0	0.6	-0.4
Scheme 8b			
Relative energy (eV)	0	0.4	-1.3

would then proceed between adsorbed pyridine and surface hydrogen species as discussed previously (Table 6).

When adjacent Ni–H groups on the Ni-edge surface are present, gas-phase pyridine may react with two Ni–H groups to form DHpyridine. Table 8 shows the activation energies and reaction energies for the formation of 2,3-DHpyridine and 1,4-DHpyridine. In Scheme 8a, pyridine reacts with two surface Ni–H to form 2,3-dihydropyridine, which requires an activation energy of 0.6 eV. The bond distance between C₂ and C₃ (1.40 Å) is shorter than the distance between the Ni–H pair (3.18 Å), and in the transition state the two surface hydrides have to bend to match the C₂–C₃ bond distance. Considering the distance between the two surface hydrides and the negative charge on the nitrogen atom, an additional path (Scheme 8b) was also investigated, where the two hydrides are added to the pyridinic nitrogen and C₄ atoms (N–C₄ distance: 2.80 Å). Following Scheme 8b, the reaction requires an activation of 0.4 eV with a large negative reaction energy (–1.3 eV) due to the strong adsorption of the product on the NiMoS catalyst surface.

In summary, E-R reactions between gas-phase pyridine and surface hydrogen species require very low activation energies; therefore, they would not be the rate-determining steps in the HDN of pyridine.

3.3. Hydrogenation of pyrrole

3.3.1. Energetics of noncatalytic pyrrole hydrogenation

Table 9 summarizes the relative energies of possible intermediate species in the hydrogenation of pyrrole with gas-phase pyrrole and molecular hydrogen as energetic references. For monohydrogenation, the energetically preferred location for the first hydrogen addition is the α -carbon (C₂) relative to pyrrolic nitrogen. For dihydropyrroles, 2,3-dihydropyrrole (2,3-DHpyrrole) is much more stable than 3,4-DHpyrrole. The first and third steps of hydrogenation are endothermic processes, and the addition of two or four hydrogen atoms is exothermic. As in the hydrogenation of pyridine, the addition of the first hydrogen to pyrrole is

Table 9
Relative energies of gas-phase pyrrole hydrogenation with pyrrole and molecular hydrogen as energetic references

State of pyrrole	Relative energy (eV)
Pyrrole	0
Monohydropyrrole	
2-MHpyrrole	0.97
3-MHpyrrole	1.35
Dihydropyrrole	
2,3-DHpyrrole	–0.20
3,4-DHpyrrole	0.86
2,3,4-Trihydropyrrole	0.13
2,3,4,5-Tetrahydropyrrole	–1.40

the most difficult step, and molecular hydrogen dissociation is required for hydrogenation to occur noncatalytically.

3.3.2. Mechanism and energetics of catalytic pyrrole hydrogenation on the Ni-edge

The side-on adsorption of pyrrole on the Ni-edge surface changes the structure of pyrrole and yields an adsorption energy of about –0.7 eV (Table 3). Therefore, it is possible that the adsorption would facilitate hydrogenation on the catalyst surface. As before, two types of reaction mechanisms for the first-step hydrogenation of pyrrole on the Ni-edge surface are discussed in the following sections: the L-H mechanism between adsorbed hydrogen and adsorbed pyrrole, and the E-R mechanism between adsorbed hydrogen species and gas-phase pyrrole.

Table 10 shows three pathways for reactions between adsorbed hydrogen and an adsorbed pyrrole molecule. For monohydrogenation, the α -carbon atoms (C₂ and C₅) that bond to the nitrogen atom are always more active than the other two β -carbon atoms (C₃ and C₄). For these three paths, the hydrogenation product is 2-MHpyrrole, and the formation of 3-MHpyrrole always requires a much higher activation energy. There are different types of hydrogen species on the Ni-edge surface that may facilitate pyrrole hydrogenation. In Scheme 10a, the source of hydrogen for the

Table 10

Activation and reaction energies of various reaction paths for the monohydrogenation of adsorbed pyrrole via the Langmuir–Hinshelwood mechanism

Reaction path	Reactant	Transition state	Product
Scheme 10a			
Relative energy (eV)	0	1.6	0.6
Scheme 10b			
Relative energy (eV)	0	1.4	0.2
Scheme 10c			
Relative energy (eV)	0	1.0	-0.02

Table 11

Activation and reaction energies of various reaction paths for dihydrogenation of pyrrole via the Eley–Rideal mechanism

Reaction path	Reactant	Transition state	Product
Scheme 11a			
Relative energy (eV)	0	0.1	-1.0
Scheme 11b			
Relative energy (eV)	0	0.1	-0.9

first-step monohydrogenation is from adsorbed H_2S , which requires an activation energy of 1.6 eV. In [Scheme 10b](#), monohydrogenation occurs between the adsorbed Ni–H and adsorbed pyrrole, which requires an activation energy of 1.4 eV. In [Scheme 10c](#), the hydrogen source is from an –SH group at the basal plane, which requires an activation energy of 1.0 eV.

The reaction path involving adsorbed H_2S ([Scheme 10a](#)) requires a higher activation energy than other reaction paths, which is in contrast to the hydrogenation of pyridine. These results indicate that a higher ratio of H_2S to H_2 in HDN reactions would benefit the hydrogenation of pyridine over pyrrole on the Ni-edge surface. The direct reaction between a Ni–H and an adsorbed pyrrole ([Scheme 10b](#)) requires a higher activation energy than the reaction between an –SH group at the basal plane and the adsorbed pyrrole ([Scheme 10c](#)). The hydrogen atom of a Ni–H first migrating to a sulfur atom and then reacting with the adsorbed pyrrole has a lower activation energy path than it would when directly reacting with pyrrole.

The energetics for several E–R reaction paths that involve surface hydrogen species and gas-phase pyrrole are presented in [Table 11](#). When there are two adjacent Ni–H groups available on the surface, the formation of dihydropyrrole is possible by the simultaneous addition of two hydrogen atoms to a pyrrole molecule. In [Scheme 11a](#), the two hydrogen atoms are added to C_2 – C_3 to form 2,3-DHpyrrole. The C_2 – C_3 bond length (1.38 Å) is much shorter than the distance of the surface Ni–H pair (3.18 Å). Thus, the Ni–H groups have to bend significantly to form two C–H bonds simultaneously with C_2 and C_3 atoms. When the hydrogen atoms are added to pyrrole at C_2 – C_4 or C_2 – C_5 , the carbon–carbon bond distance (2.26 Å) is closer to the surface Ni–H pair distance (3.18 Å), and only slight bending of the Ni–H groups is needed. When C_2 and C_4 are simultaneously approaching the Ni–H groups, only the C_2 atom forms a bond with one hydride (not shown). However, when C_2 and C_5 are simultaneously approaching the Ni–H groups, the two hydrides form C–H bonds producing 2,5-DHpyrrole, as shown by [Scheme 11b](#). These reaction paths have very low activa-

tion energies ($E_a \approx 0.1$ eV). This type of mechanism, however, can only be possible at very high partial pressures of hydrogen and low partial pressures of pyrrole.

3.4. Implications to hydrotreating

By comparing the results for pyridine (Tables 6 and 8) and pyrrole (Tables 10 and 11), one can note that pyrrole and pyridine would respond to changes in reaction conditions differently. Increasing the partial pressures of H_2S in the gas phase would increase the concentration of adsorbed H_2S on the catalyst surface and thus favor the lower activation paths (Scheme 6a) for pyridine and higher activation energy paths for pyrrole (Scheme 10a). On the other hand, increasing the partial pressure of hydrogen would increase the concentration of surface Ni–H and –SH, thereby favoring the higher activation paths (Schemes 6c and d) for pyridine and lower activation energy paths for pyrrole (Schemes 10b and c). At extremely low partial pressures of nitrogen compounds and very high partial pressure of hydrogen, reactions could follow an E-R mechanism between gas-phase molecules and adsorbed hydrogen species. Along such a mechanism, pyrrole hydrogenation does not have an activation energy barrier, whereas pyridine hydrogenation still possesses a small activation energy barrier. Following this mechanism, the rate-determining step would then be the dissociation of hydrogen on the catalyst surface.

4. Conclusions

The most stable configuration for pyridine on the Ni-edge surface is the end-on adsorption through Ni–N bonding. The reaction between adsorbed pyridine and surface hydrogen species requires lower activation energy when the hydrogen is from an adsorbed H_2S compared with Ni–H or an –SH group at the basal plane. For pyrrole, the most stable configuration on the Ni-edge surface is through the bonding of an α -carbon to a nickel site. The activation energy of the reaction pathway involving an –SH group at the basal plane is lower than that of other reaction pathways involving adsorbed H_2S or Ni–H. Reaction pathways involving gas-phase pyridine or pyrrole and surface hydrogen species require very low activation energies; thus the dissociation of hydrogen on the catalyst surface would be the rate-determining step. Because of the strong adsorption of the nitrogen-containing molecules on the catalyst surface, the L-H mechanism would dominate at normal conditions. However, the E-R mechanism might be significant at very low partial pressures of nitrogen-containing compounds and very high partial pressures of hydrogen. Therefore, in a very

carefully designed experiment one should be able to observe a change in the intrinsic activation energies for the hydrogenation of pyridine and pyrrole with reaction conditions due to the change in reaction mechanisms.

Acknowledgments

This work is supported by Syncrude Canada Ltd. and the Natural Sciences and Engineering Research Council (NSERC) under grant no. CRDPJ 261129.

References

- [1] R. Prins, V.H.J. de Beer, G.A. Somorjai, Catal. Rev.-Sci. Eng. 31 (1989) 1.
- [2] H. Topsøe, B.S. Clausen, F.E. Massoth, Hydrotreating Catalysis, Science and Technology, vol. 11, Springer, Berlin, 1996.
- [3] H. Topsøe, B.S. Clausen, R. Candia, C. Wivel, S. Morup, J. Catal. 68 (1984) 433.
- [4] J.V. Lauritsen, S. Helveg, E. Lægsgaard, I. Stensgaard, B.S. Clausen, H. Topsøe, F. Besenbacher, J. Catal. 197 (2001) 1.
- [5] L.S. Byskov, J.K. Nørskov, B.S. Clausen, H. Topsøe, J. Catal. 187 (1999) 109.
- [6] P. Raybaud, J. Hafner, G. Kresse, S. Kasztelan, H. Toulhoat, J. Catal. 190 (2000) 128.
- [7] H. Schweiger, P. Raybaud, H. Toulhoat, J. Catal. 212 (2002) 33.
- [8] M. Sun, A.E. Nelson, J. Adjaye, J. Catal. 226 (2004) 32.
- [9] M. Sun, J. Adjaye, A.E. Nelson, Appl. Catal. A 263 (2004) 131.
- [10] G. Perot, Catal. Today 10 (1991) 447.
- [11] R. Prins, Adv. Catal. 46 (2001) 399.
- [12] V.H. Grassian, E.L. Muetterties, J. Phys. Chem. 90 (1986) 5900.
- [13] J.C. Serafin, C.M. Friend, J. Phys. Chem. 93 (1989) 1998.
- [14] W.A. Abdallah, A.E. Nelson, M.R. Gray, Surf. Sci. 569 (2004) 193.
- [15] G. Tourillon, S. Raaen, T.A. Skothem, M. Sagurton, R. Garrett, G.P. Williams, Surf. Sci. 184 (1987) L345.
- [16] G.R. Schoofs, J.B. Benziger, Surf. Sci. 192 (1987) 373.
- [17] C.J. Baddeley, C. Hardacre, R.M. Ormerod, R.M. Lambert, Surf. Sci. 369 (1996) 1.
- [18] M. Sun, A.E. Nelson, J. Adjaye, Catal. Today (2004), in press.
- [19] B. Delley, J. Chem. Phys. 113 (2000) 7756.
- [20] A.D.J. Becke, Chem. Phys. 88 (1988) 2547.
- [21] J.P. Perdew, Y. Wang, Phys. Rev. B 45 (1992) 13244.
- [22] M. Dolg, U. Wedig, H. Stoll, H. Preuss, J. Chem. Phys. 86 (1987) 866.
- [23] A. Bergner, M. Dolg, W. Kuechle, H. Stoll, H. Preuss, Mol. Phys. 80 (1993) 1431.
- [24] S. Bell, J.S. Crighton, J. Chem. Phys. 80 (1984) 2464.
- [25] S. Fischer, M. Karplus, Chem. Phys. Lett. 194 (1992) 252.
- [26] G. Henkelman, H. Jonsson, J. Chem. Phys. 113 (2000) 9978.
- [27] M. Sun, A.E. Nelson, J. Adjaye, J. Mol. Catal. 222 (2004) 243.
- [28] J.F. Cocchetto, C.N. Satterfield, Ind. Eng. Chem., Proc. Des. Dev. 15 (1976) 272.
- [29] R.T. Hanlon, Energy Fuels 1 (1987) 424.
- [30] V. Morávek, Appl. Catal. 66 (1990) 257.
- [31] J.A. Anabtawi, R.S. Mann, K.C. Khulbe, J. Catal. 63 (1980) 456.
- [32] J. Sonnemans, J.M. Janus, P. Mars, J. Phys. Chem. 80 (1976) 2107.